Pergamon

Int. J. Heat Mass Transfer. Vol. 37, No. 12, pp. 1687–1697, 1994

0017-9310/94 $7.00 + 0.00

0017-9310(94)E0005-F

Air jet impingement heat transfer at low nozzle–plate spacings

D. LYTLE and B. W. WEBB†

Department of Mechanical Engineering, Brigham Young University, Provo, UT 84602, U.S.A.

(*Received* 9 *September* 1993 *and in final form* 4 *January* 1994)

Abstract—The local heat transfer characteristics of air jet impingement at nozzle–plate spacings of less than one nozzle diameter have been examined experimentally using an infrared thermal imaging technique. Fully-developed nozzles were used in the study. The flow structure was investigated using laser-Doppler velocimetry and wall pressure measurements. The stagnation Nusselt number was correlated for nozzle–plate spacings of less than one diameter. The customary Nusselt number dependence on $Re^{1/2}$ for impinging jet transport was observed. A power-law relationship between Nusselt number and nozzle–plate spacing of the form $Nu_0 \sim (z/d)^{-0.288}$ observed experimentally is explored from theoretical considerations. The effects of accelerating fluid between the nozzle–plate gap as well as a significant increase in local turbulence leads to substantially increased local heat transfer with decreased nozzle–plate spacing. A stagnation point minimum surrounded by an inner and outer peak in the local heat transfer was observed for nozzle–plate spacings less than $z/d = 0.25$. These primary and secondary maxima are explained by accelerated radial flow at the exit of the jet tube and an observed local maximum in the turbulence, respectively. These conclusions are drawn from observations made relative to the turbulent flow structure and wall pressure measurements. The outer peak in local Nusselt number was found to move radially outward for larger nozzle–plate spacings and higher jet Reynolds numbers.

INTRODUCTION

MANY APPLICATIONS in industry require localized heating or cooling. An effective way to accomplish this is through the use of impinging gas jets. Industrial uses of impinging air jets include tempering of glass, drying of paper and textiles, and the cooling of metal sheets, turbine blades, and electronic components. The objective of this investigation is to characterize the transport characteristics of an axisymmetric impinging air jet at a nozzle–plate spacing of less than one diameter. At low nozzle–plate spacings impinging gas jets exhibit behavior not evident at higher spacings. At spacings less than $z/d = 0.25$, for circular nozzles, the air is forced to accelerate while exiting under the nozzle wall.

Due to the many industrial uses for impinging jets extensive prior research has been conducted to understand their heat/mass transfer characteristics. The results from this research have been summarized in recent reviews [1, 2]. Martin also provides a comprehensive review with an emphasis on the engineering applications of impinging jets [3]. It is not the intent of this review to repeat the work accomplished by these reviewers, but rather to focus on previous experimental and theoretical work dealing with low nozzle–plate spacings.

An important contribution of prior research on submerged gas jets is the observation that for nozzle–plate spacings greater than approximately four nozzle diameters, the maximum heat transfer occurs at the stagnation point of the jet [4]. It has also been observed that at close nozzle–plate spacings a local minimum in heat transfer develops at the stagnation point and two distinct peaks are seen in the radial direction. The first peak corresponds to the maximum heat transfer and occurs in an annular region near the nozzle wall, 0.5 nozzle diameters ($r/d = 0.5$). Gardon and Akfirat [4] suggested that this inner peak may be due to accelerating flow at nozzle–plate spacings below $z/d = 0.25$ (circular nozzles), and due to a local thinning in the boundary layer as proposed theoretically by Kezios [5], for larger nozzle–plate spacings. Pamadi and Belov [6] refuted the idea of local thinning of the boundary layer, and through the use of a semi-empirical turbulent numerical model proposed that the inner peaks be attributed to the non-uniform, mixing-induced turbulence in the developing jet. Pamadi and Belov suggest that while the jet is impinging within the length of its potential core ($z/d < 5$–8), the annular region of mixing-induced turbulence penetrates the boundary layer, causing the increased heat transfer

† To whom correspondence should be addressed.

NOMENCLATURE

d	nozzle diameter	r	radial location, measured from the stagnation point
k	thermal conductivity		
L	nozzle length	Re	nozzle Reynolds number, $v_j d/\nu$
Nu	local Nusselt number, equation (1)	T_j	jet exit temperature
Nu_0	stagnation Nusselt number	T_s	local heated surface temperature
$\overline{Nu}$	average Nusselt number, equation (3)	u	local mean radial velocity
P	local wall gage pressure	u'	local RMS velocity fluctuation
P_0	stagnation point gage pressure	v_j	average velocity in the nozzle tube
q_{conv}	convective heat flux imposed at heating plate	y	normal distance from the heated plate
		z	nozzle–plate spacing.

at $r/d = 0.50$–0.60. The second peak in local Nusselt number, $r/d = 1.5$–2.5, was attributed to transition from a laminar to a turbulent boundary layer in the spreading wall jet [4]. This explanation of the outer peak is also supported by others [6–8].

Scholtz and Trass [9] investigated, both numerically and experimentally, laminar impingement mass transfer with a nonuniform laminar velocity profile for nozzle–plate spacings ranging from 0.05 nozzle diameters to 6 nozzle diameters. It was concluded that the impingement mass transfer was independent of nozzle-to-plate spacing within the range of 0.5 to 6.0 nozzle diameters for $500 \leqslant Re \leqslant 1970$. For spacings less than 0.25 nozzle diameters, the effect of fluid acceleration between the nozzle wall and impingement plate was seen, and the mass transfer increased from the stagnation point to a peak at $r/d = 0.5$ and then decreased monotonically. At $z/d = 0.05$, the peak Sherwood number was twice that at the stagnation point. No secondary peak associated with transition was seen, which is in agreement with the data of Gardon and Akfirat [4] at low Reynolds numbers.

The majority of prior research on impinging gas jets has focused on nozzle–plate spacings much larger than one diameter. No previous quantitative work for $z/d \leqslant 0.5$ in the high Reynolds number, turbulent flow regime has been conducted. The intent of this research is to fill the void in the current impingement literature and to present a qualitative and quantitative understanding of impingement heat transfer and flow structure at low nozzle–plate spacings.

TEST APPARATUS AND METHOD

Heat transfer

To quantify the heat transfer found at nozzle–plate spacings less than one nozzle diameter, experiments were conducted for dimensionless nozzle–plate spacings of $z/d = 0.1, 0.15, 0.2, 0.25, 0.5, 0.75, 1.0$ and 6.0 for nine different Reynolds numbers ranging from 3600 to 27 600. To compare with previously published data additional experiments were conducted for $2.0 \leqslant z/d \leqslant 10.0$ for a Reynolds number of 18 400.

The experimental apparatus consists of three major components: the heated impingement plate, the nozzle and flow metering system, and the infrared camera and image diagnostic equipment, shown schematically in Fig. 1. The cooling air flows from the compressed air supply, through the pressure regulator and flow rate meter and into the nozzle which directs the air until it impinges upon the heated plate. The infrared thermal image of the heated plate is recorded by the infrared camera. Each of these components will now be described in detail.

The impingement plate, 20.32 cm long by 5.0 cm wide, was constructed of 0.051 mm thick stainless steel shim stock and attached to an aluminum bus bar at each end. A hole was drilled through the length of each bus bar, through which a steel rod was inserted, maintaining the plate and bus bar assembly vertical. The steel rods were set in holes and attached rigidly to a Lexan base, 2.54 cm thick by 68.6 cm long by 39.4 cm wide. Two large springs, insulated at their ends, were connected to the top and bottom of the bus bars, creating a moment about the axis of the steel rods and providing an even tension on the plate. The stainless steel shim stock was heated Ohmically yielding a constant heat flux. To achieve an isoflux surface, voltage from an HP 6031A DC power supply was imposed across the plate through the aluminum bus bars. A considerable voltage drop occurred across the bus bars and the power supply lines, so voltage taps were spot welded precisely 103.5 mm apart on the plate and wired to a Fluke 75 Multimeter to measure the voltage. The current was measured by the digital readout of the power supply. This configuration yielded a worst case uncertainty in the Ohmic dissipation measurement of less than 1%. The measured heat flux was corrected for losses due to radiation from both sides of the plate and for natural convection from the side opposite the impinging jet. Typically these losses were 4–7% of the total imposed heat flux. During data collection for each spacing and Reynolds number the voltage was set to furnish the highest temperature difference within a 20°C measurement range selected on the camera. The difference between the jet exit air temperature and the minimum local plate temperature typically was 9–12°C, with a worst case of 6°C.

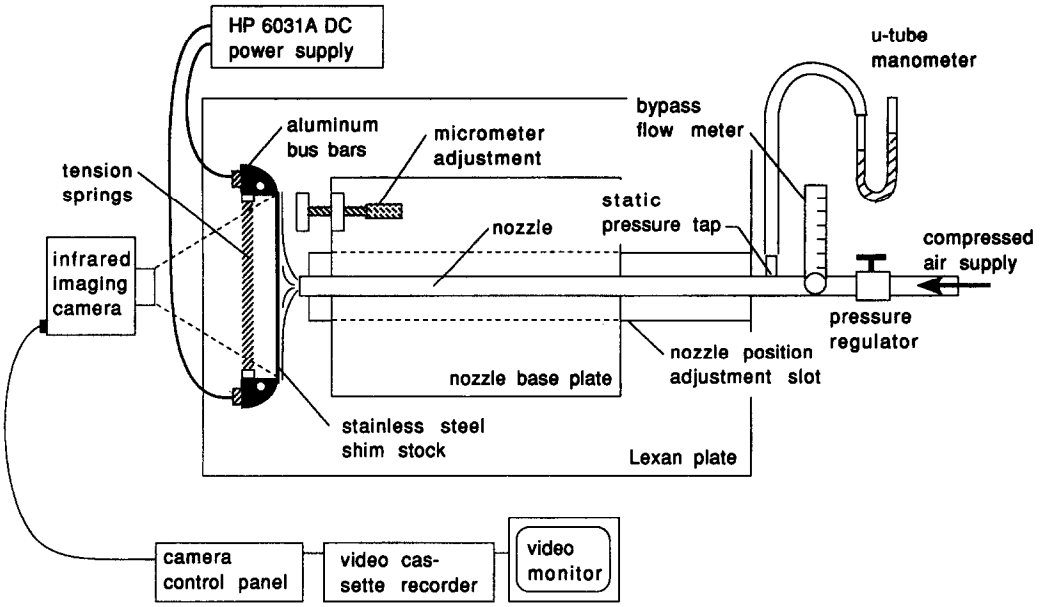

FIG. 1. Schematic of experimental apparatus.

Radial conduction in the heated plate was considered by solving numerically the one-dimensional energy equation in the plate's radial direction subject to the measured local heat transfer coefficient distributions. While this analysis does not truly reflect the conjugate nature of the problem, it gives an idea as to the magnitude of the lateral conduction in the plate. For the experimental conditions yielding the highest radial temperature gradients in the plate (highest Reynolds number and smallest nozzle–plate spacing), the analysis revealed a maximum of 3% of the imposed heat flux which was laterally conducted in the plate. For radial locations in most experiments, the lateral redistribution of energy was less than 0.5%. The lateral conduction in the heated plate was therefore neglected.

Two circular tube nozzles, 7.8 mm diameter by 61 cm long, and 10.9 mm diameter by 61 cm long, with 1.4 mm wall thickness were used, ensuring fully-developed flow over the Reynolds number range investigated. The end of each was machined perpendicular to the nozzle axis. The cooling air was supplied by a large capacity compressor and was regulated and filtered after which the volume flow rate was metered to within 5% by a calibrated rotameter.

During experimentation at close spacings ($z/d \leqslant 0.25$) when the nozzle was moved relative to the plate, the pressure drop and hence, the flow rate changed drastically. A consequence of this was a reduction in flow rate with a decrease in nozzle–plate spacing, for a fixed pressure regulator setting. Thus, care was taken to recheck, and change if necessary, the measured volume flow rate after each spacing adjustment.

The Inframetrics Model 600 Infrared Imaging Radiometer was used to collect the local temperature data. The infrared camera was positioned on the side of the heated plate opposite the impinging nozzle, and non-intrusively detected the radiosity of the impingement plate. The side of the impingement plate facing the camera was painted flat black to increase the emitted energy from the heated plate, and the paint layer was measured to be less than 0.013 mm thick. A one-dimensional energy balance across the heated plate–paint composite layer revealed that the difference between measured temperature on the back side of the plate and that on the impingement surface was never more than 0.05°C over the full range of experimental conditions studied. The local temperature measured on the back side was thus assumed to be identical to that on the impingement surface.

With the detected radiosity, and by knowning the emissivity of the plate and surrounding temperature, the infrared camera determines the local temperature with its internal calibration table. The emissivity of each side of the plate was measured with the imaging camera and was found to be 0.95 and 0.17 for the painted and unpainted surfaces, respectively. The two-dimensional thermal image on the heated plate is detected by the camera and recorded onto video tape using a conventional video cassette recorder (VCR). While recording, image averaging was used to reduce the random noise content of the thermal images. A video monitor was cabled to the camera, via the VCR, so the temperature field could be viewed during the data runs. From the video tape, using a commercial thermal image processing system, the local temperatures are extracted and used to calculate the heat transfer coefficients of the impinging jet. The thermal image processing system is a computer hardware and software interface that allows the playback, analysis and storage of recorded thermal images.

A critical criterion in the design of the apparatus was accurate measurement of the nozzle–plate spacing. To accomplish this a groove was machined through the center of the Lexan plate, 7.93 mm deep and 50.8 mm wide, normal to the impingement plate. A mating tongue was machined in the moveable plate upon which the nozzle was connected (nozzle base plate). The nozzle base plate rests upon, and moves relative to the Lexan plate, allowing the nozzle to slide back and forth normally with respect to the heater apparatus. At spacings of less than one diameter adjustment between the nozzle and plate was made by a micrometer attached to the nozzle base plate. When using the micrometer it was necessary to make a relative measurement. The nozzle was brought flush and square to the plate and the micrometer reading was recorded as a reference. All subsequent positional measurements were made relative to this reference. This worked well for all tests except those above Reynolds numbers of 12 000. For these higher Reynolds numbers and for the lower nozzle–plate spacings, $z/d = 0.1, 0.15, 0.2$, a slight deflection in the plate was noted due to the pressure of the impinging fluid. The deflection was measured using a sensitive dial gage indicator, then subtracted from the ideal distance to achieve a corrected nozzle–plate spacing. For the majority of experimental conditions the deflection was less than 0.254 mm. A maximum deflection of 0.96 mm was observed at the highest Reynolds number and lowest nozzle–plate spacing. In all experiments the nozzle–plate spacing was corrected for the pressure-induced deflection. The angle made by the deflected heater plate with respect to the undeflected position was always less than 0.3 degrees. The slight curvature of the heated plate at the stagnation point is therefore considered negligible. At the larger spacings adjustment of the nozzle–plate gap was accomplished by measuring the desired distance with a Vernier caliper, then sliding the nozzle base plate with respect to the heated plate to match the distance.

Some prior work on jet impingement heat transfer with gas jets has employed the local adiabatic wall temperature in defining the local Nusselt number [8, 10–12], while others have used the jet exit temperature [4, 6, 7, 9]. The jet exit temperature was used to calculate the local heat transfer coefficients in this study. Nozzle Reynolds numbers were maintained below 28 000 in this investigation, so such effects were considered minimal. The maximum Mach number in the nozzle and nozzle–plate gap, respectively, was 0.16 and 0.4. Indeed, the Mach number in the nozzle–plate gap exceeded 0.3 in only two experiments. Compressibility effects were thus considered negligible.

The jet exit air temperature was measured by recording the thermal image of the heater foil with the air impinging but with no heat flux imposed. The heat transfer coefficient is sufficiently high and the thermal interaction of the plate with the environment is sufficiently low under these conditions to permit the assumption that the (unheated) foil temperature is identical to the jet exit air temperature. The nozzle–plate spacing was adjusted until the measured temperature in the stagnation zone (which is assumed identical to the jet exit air temperature) was no longer dependent on z/d. At this point entrainment and other effects did not influence the measurement. Local temperature differences needed to calculate the local heat transfer coefficient were then determined by subsequently imaging the plate with heating imposed. Calibration of the infrared camera using isothermal targets showed good accuracy in absolute temperature (less than 0.5°C difference between IR camera and thermocouple measurements). It is true, however, that absolute temperature measurement using infrared radiometry can suffer from considerable systematic error. The two-image differencing technique used here effectively eliminates the systematic error for the measured temperature *differences*, $\Delta T = T_s - T_j$. The temperature differences used in the determination of the heat transfer coefficient were estimated to be accurate to 0.3°C.

The warming or cooling effect of the jet after exiting the nozzle due to entrainment of the ambient air was minimal for two reasons. First, as suggested by Striegl and Diller [13, 14], the impinging air temperature was very near the ambient air temperature for all experiments, and second, the low nozzle–plate spacings would not allow adequate distance for the ambient air to be entrained into the potential core.

With this experimental arrangement and procedure the uncertainty ranged from 2–9% in the Nusselt number calculation and 3–8% in the Reynolds number calculation. Velocity measurements are estimated accurate to 5%. Details of the uncertainty analysis may be found in ref. [15].

The local temperature data recorded by the infrared radiometer were reduced to local and average Nusselt numbers for all configurations studied. The local Nusselt number was calculated by

$$Nu = q_{\text{conv}} d / k(T_s - T_j) \tag{1}$$

where q_{conv} is the imposed Ohmic heat flux, corrected for radiation and natural convection. Local radiation corrections were made for both the front (impingement) and back (IR-imaged) sides of the foil, while natural convection losses on the back side were made assuming laminar free convection. The combined losses amounted to 4–7% of the imposed Ohmic flux. The average Nusselt number for a constant heat flux surface is based on the average temperature difference:

$$\overline{T_s - T_j} = \frac{2}{r^2}\int_0^r (T_s - T_j) r' \, dr'. \tag{2}$$

In practice, the integral of equation (2) was evaluated using the trapezoidal rule, after which the average Nusselt number was determined at a specific radial location from its definition

$$\overline{Nu} = q_{conv} d/k(\overline{T_s - T_j}). \quad (3)$$

Hence, from the knowledge of the average Nusselt number and imposed surface heat flux, the average heated surface temperature difference may be calculated.

Flow structure

Radial velocity measurements were made with a laser-Doppler velocimeter. The system was a TSI Model 1980B used in conjunction with a 5 W Spectra-Physics argon ion laser. The LDV was operated in backscatter mode, and was traversed via a computer-controlled traversing table to within ± 0.1 mm. Frequency shifting was used to improve the data rate and to reduce the fringe bias. The same impingement apparatus used for the heat transfer measurements was employed in the velocity measurements with the exception that a plexiglas plate was used as the impingement surface rather than the stainless steel shim stock, again, to alleviate a z/d correction due to pressure-induced deflection of the stainless steel foil. A section of stainless steel shim stock was attached to the plexiglass impingement plate to ensure that the surface roughness was identical for the heat transfer and velocity measurements. The flow was seeded well upstream of the nozzle exit with a salt-water solution from a Fairchild six-jet atomizer. The atomizer evaporated the water leaving micron-sized salt particles. The manufacturer-supplied atomizer documentation indicated that such a solution produced seeding particles of order 1 μm.

All velocity measurements were made with locations determined relative to the impingement plate. The wall location was found by incrementing the LDV diagnostic volume systematically closer to the plate until the oscilloscope output displayed only the shift frequency. Turbulence statistics determined for increasing numbers of points revealed that accurate mean and RMS velocity data were found by collecting 5000 instantaneous points. Velocity measurements were made for z/d spacings of 0.1, 0.2, and 0.5, and for Reynolds numbers of 7800 and 11 000 for the 10.9 mm diameter nozzle. Two types of velocity measurements were made: (1) radial traverses at a fixed distance from the plate, and (2) velocity maps, made by measuring profiles normal to the plate at several radial locations.

Wall pressure

Local wall pressure measurements were made to assist in the understanding of local heat transfer and flow structure measurements. These measurements were made by replacing the stainless steel heater foil with a plexiglass plate. A small hole, approximately 0.5 mm in diameter was drilled in the plate, which was then connected via tubing to an MKS Baratron for pressure measurements. For some measurements, the measured pressure (relative to atmospheric pressure) was outside the range of the two sensing heads (1 and 10 mm Hg, respectively) of the Baratron. Under these conditions, a combination of U-tube and inclined manometers were used to determine the local wall pressure. The horizontal jet was fixed relative to the measurement plate, and the plate was traversed using a machinists's gage with micrometer adjustment. This provided relative radial location measurement to within ± 0.1 mm. The nozzle–plate spacing was determined using the same technique as for the heat transfer measurements. The stagnation point was determined in these measurements by traversing radially from one side of the stagnation zone to the other, and using symmetry to locate the $r = 0$ point. These wall pressure measurements were made for two nozzle diameters ($d = 6.9$ and 13.9 mm) and for two Reynolds numbers in the nozzle–plate spacing range $0.1 \leqslant z/d \leqslant 5.0$

EXPERIMENTAL RESULTS AND DISCUSSION

Flow structure

Figures 2(a) and 2(b) show the radial velocity and RMS velocity profiles non-dimensionalized by the mean jet velocity in the tube for $z/d = 0.5$, 0.1 and $Re = 11\,000$. The distance from the plate for each measurement, y, has been normalized by the nozzle–plate spacing, z. The position $y/z = 1.0$ therefore corresponds to a measurement taken at a distance from the impingement plate which corresponds to the nozzle–plate spacing. At the stagnation point essentially no radial velocity component can be seen; the flow is forced to stagnate and accelerate radially outward. At $r/d = 0.5$ the flow continues to be deflected by the impingement surface and reaches a maximum velocity at $r/d = 1.0$. At further radial positions the boundary layer continues to develop and thicken as the velocity decelerates. Significantly higher radial velocities are observed near the nozzle exit for the smaller nozzle–plate spacing ($z/d = 0.1$); the radial velocity component reaches magnitudes more than double the mean velocity in the jet tube, v_j. This is consistent with global continuity considerations, which require that the average normalized velocity in the gap be $\bar{u}_{gap}/v_j = 2.5$ for $z/d = 0.1$. Recall that mean acceleration in the gap, characterized by an average gap velocity higher than the jet tube velocity ($\bar{u}_{gap} > v_j$), occurs only for $z/d \leqslant 0.25$ for axisymmetric jets. These higher velocities for the smaller nozzle–plate spacing prevail vertically from the impingement plate into what would be the freestream air above $y/z = 1.0$. This indicates that the freestream air experiences considerable motion due to entrainment and intense shear layer effects near the nozzle gap exit. By contrast, the velocities seen from the $z/d = 0.5$ configuration approach zero as $y/z \to 1$ at low r/d, suggesting a relatively undisturbed freestream. It should be noted that measurements at increasingly large y/z (far from the plate) were limited

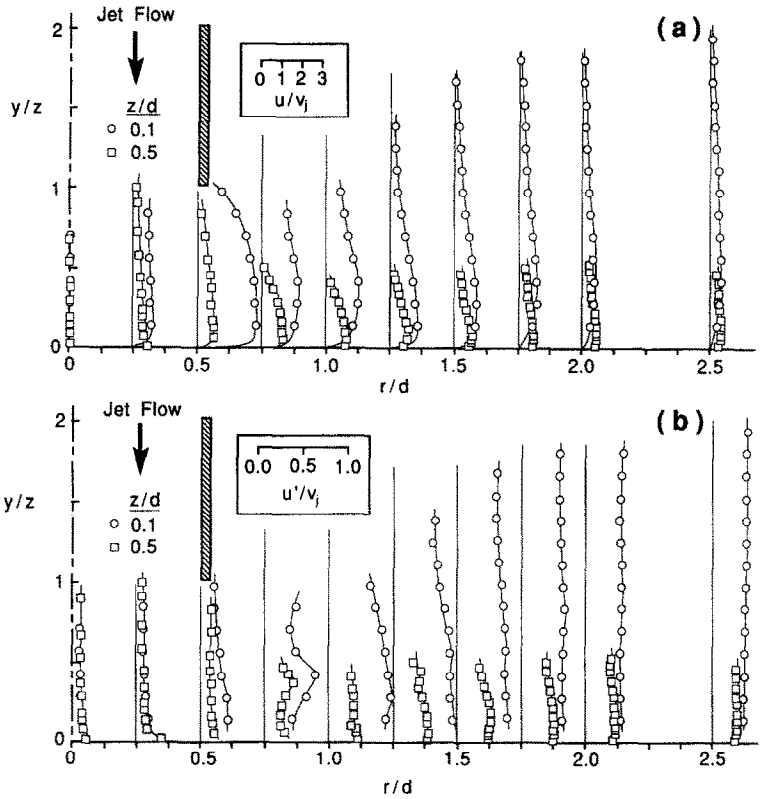

FIG. 2. Measured distributions of mean velocity and RMS velocity fluctuations for $Re = 11\,000$.

by reduced seed levels, since more unseeded ambient air was entrained into the flow in this region.

The profiles of the normalized RMS turbulence (u'/v_j) corresponding to the mean flow structure of Fig. 2(a) are found in Fig. 2(b). It is noted that RMS turbulence levels are relatively high even directly under the jet; the values of u'/v_j on the stagnation line were approximately 10%. Apparently the deceleration of the flow results in higher unsteadiness here than might be expected. Turbulence data for both nozzle–plate spacings suggest high shear interaction with the radially flowing jet near $r/d \approx 0.75$, as evidenced by the local maximum in u'/v_j at approximately $y/z = 0.4$. Presumably, it is here that the jet flow interacts most significantly with the stagnant ambient air. The normalized RMS velocity is considerably higher in this region for the $z/d = 0.1$ nozzle–plate spacing configuration. The accelerated flow exiting radially from the gap interacts more significantly with the free-stream air for this case. This shear layer interaction is believed to be the cause of a significant rise in the levels of local turbulence for small z/d, to be seen in what follows.

Also of note in Fig. 2(b) is the fact that the normalized RMS turbulence for both z/d configurations increase with r/d until a maximum is reached, followed by a decrease thereafter. As will be seen later, this increase in turbulence level has a profound effect on the local heat transfer. It is also noted that the levels of RMS turbulence for the $z/d = 0.5$ data approach those for the $z/d = 0.1$ configuration at large r/d. The shear layer separating the radial jet and the near-stagnant ambient thickens with r/d for both nozzle–plate configurations until their turbulence characteristics are nearly identical.

Wall pressure measurements under the jet are reported in Fig. 3 for two different nominal Reynolds numbers and four different nozzle–plate spacings. The local wall gage pressure for each data set has been normalized by the corresponding stagnation point gage pressure, P_0, to facilitate comparison of the different experimental conditions. The pressure data reveal a zone of nearly constant pressure (at the stagnation pressure) which grows for decreasing nozzle–plate spacing; the $z/d = 5.0$ pressure data exhibit a gradual fall from the stagnation pressure to near-ambient pressure. By contrast, the lower z/d data show a sharp drop in P/P_0 near $r/d = 0.5$. The radial location where the decline in pressure occurs increases for higher Reynolds numbers (seen by comparing the $Re = 6800$ and 13 600 data for $z/d = 0.1$, $d = 13.9$ mm). Also of interest is the drop in pressure below atmospheric which can occur for higher Reynolds numbers at low nozzle–plate spacings. This occurs beyond the nozzle edge, at approximately $r/d = 0.7$. This is believed to be due to the *vena contracta* effect as the mean flow accelerates through the nozzle–plate gap for $z/d = 0.1$.

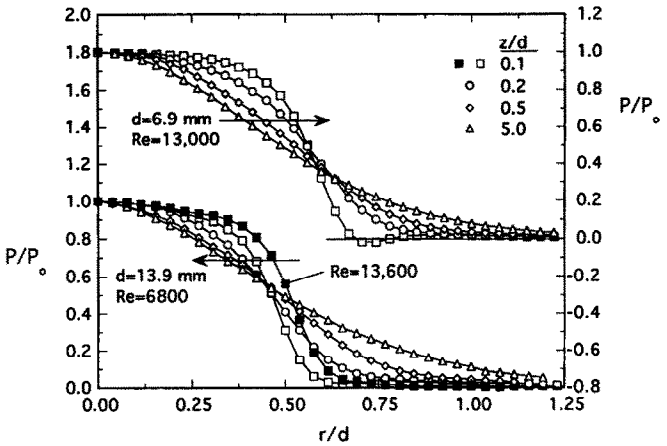

FIG. 3. Wall static pressure measurements as a function of radial position.

Heat transfer

As a validation exercise, stagnation point heat transfer coefficients from the present study were compared with previously reported results in the nozzle–plate spacing range $1 \leqslant z/d \leqslant 10$ and for Reynolds numbers in the range $3700 \leqslant Re \leqslant 30\,000$. For a given z/d, the Reynolds number variation from this study agreed with previous results [3, 7, 16] with an average deviation of 14%. Differences are attributed to different hydrodynamic conditions at the nozzle exit [17]. For a given Reynolds number, the variation of Nu_0 with z/d from this study agreed with a correlation of prior work [3] to within 10%. Details of this comparison with previous work may be found elsewhere [15].

Measured data for the stagnation Nusselt number are shown in Fig. 4. For nozzle–plate spacings less than one nozzle diameter ($z/d \leqslant 1.0$), a least-squares correlation of the data was determined of the form

$$Nu_0 = 0.726Re^{0.53}(z/d)^{-0.191}. \quad (4)$$

The correlation of equation (4) is shown in Fig. 4 with the experimental data. Equation (4) represents the data with average and maximum error of 5 and 21%, respectively. If only the data for nozzle–plate spacings

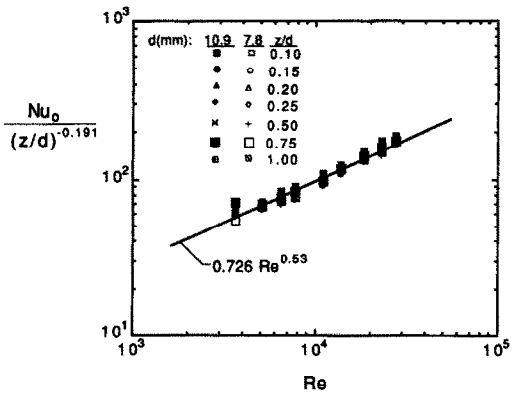

FIG. 4. Variation of the stagnation Nusselt number with Reynolds number.

at or below $z/d = 0.5$ are included in the least-squares regression, the correlation becomes

$$Nu_0 = 0.663Re^{0.53}(z/d)^{-0.248} \quad (5)$$

with slightly better accuracy. Further increases in the absolute magnitude of the exponent on z/d are seen if the least-squares regression is performed by systematically excluding experimental data at higher nozzle–plate spacings. Both equations reveal the usual dependence of Nusselt number on $Re^{1/2}$ for impinging jets as is reported elsewhere [3]. Also of note is the increase in Nu_0 with decreasing z/d according to a power law relationship. Equation (4) reveals that Nu_0 increases by 60% as z/d is decreased from 1.0 to 0.1. There is a theoretical basis for the Reynolds number and z/d relationships. The heat transfer coefficient for a theoretical solution for a laminar jet of infinite extent is [18]

$$h = 0.44\sqrt{(3)}k(c/v)^{1/2}. \quad (6)$$

Theory reveals that the heat transfer coefficient for the infinite stagnation flow is radially constant. The constant c in equation (3) is the freestream velocity gradient, $c = \partial U/\partial r$, and is determined from the potential flow in the freestream for the infinite jet. As an approximation, one may extend equation (6) to the finite jet studied here, and determine c from the application of continuity at the gap (for low z/d) as

$$c = \frac{\bar{u}_{gap}}{(d/2)} = \frac{v_j}{2z} \quad (7)$$

where $\bar{u}_{gap}$ is the mean radial velocity in the nozzle–plate gap. While a better estimate of the radial velocity gradient might be found from a potential flow solution, the approximation given by equation (7) will serve to illustrate the scaling of Nusselt number with nozzle–plate spacing. Substituting the expression for the stagnation point radial velocity gradient given by equation (7) into equation (6), and non-dimensionalizing yields

$$\frac{Nu_0}{Re^{1/2}} = 0.539(z/d)^{-1/2}. \quad (8)$$

The approximation for the velocity gradient given in equation (7) is expected to be more accurate as the nozzle–plate spacing is decreased, since there will be less spatial variation in radial velocity across the gap for smaller z/d. The approximate theoretical relationship for the stagnation Nusselt number given by equation (8) illustrates the power-law Reynolds number and z/d dependence observed in the experimental data. The theoretical dependence on z/d, however, is more pronounced. If one forces the $Nu_0 \sim Re^{1/2}$ relationship in the least-squares regression of the experimental data for $z/d \leqslant 0.25$, the empirical correlation becomes

$$\frac{Nu_0}{Re^{1/2}} = 0.821(z/d)^{-0.288}. \quad (9)$$

Figure 5 illustrates the experimental data plotted against the approximate theoretical result of equation (8), as well as the least-squares correlation of equation (9). The approximate theory predicts the stagnation Nusselt number to within 13% for $z/d \leqslant 0.25$ (the range of validity of the empirical correlation of equation (9)). Note that the theory proposed shows improved accuracy as z/d is reduced, consistent with the expectation stated previously that the approximation for the velocity gradient, c, is better for smaller nozzle–plate spacings. Figure 5 also reveals that the experimental data are generally higher than the theory, perhaps due to the influence of turbulent transport in the experimental work; RMS velocity fluctuations at the stagnation zone were seen to be approximately 10% at $r/d = 0$ in Fig. 2.

Local Nusselt number profiles are shown in Fig. 6 for z/d ranging from 0.1 to 6 for two Reynolds numbers. Trends observed in these data are representative of those found for other similar experimental conditions. Consider first the $Re = 23\,000$ data. At the largest spacing, $z/d = 6$, the maximum Nusselt number occurs at the stagnation point and decreases monotonically. As the nozzle–plate spacing is reduced to $z/d = 0.5$, a slight secondary local maximum (or plateau) in Nu develops at $r/d = 1.75$.

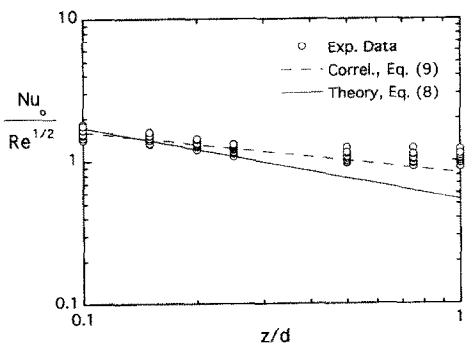

FIG. 5. Variation of experimentally determined stagnation Nusselt number with nozzle–plate spacing and comparison with approximate theoretical relationship, equation (8).

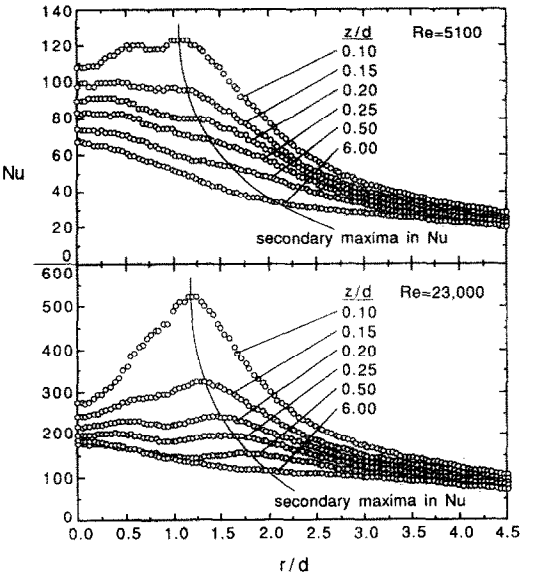

FIG. 6. Radial variation in Nusselt number with nozzle–plate spacing for two Reynolds numbers.

Otherwise, the local Nusselt numbers are nearly the same magnitude as for $z/d = 6$ despite such a large difference in nozzle–plate spacing. The stagnation point Nusselt number for $z/d = 6$ is even slightly higher than that at $z/d = 0.5$ due to a peak in turbulence at the end of the potential core for $z/d = 6$ [3]. Further decreases in nozzle–plate spacing result in a local minimum at the stagnation point and an inner local maximum in Nusselt number developing at $r/d \approx 0.5$ with further increases in the magnitude of the outer peak. In addition to the development of the inner and outer peak (or plateau), the magnitude of the Nusselt numbers at all radial locations increase considerably. As the nozzle–plate spacing is decreased to the lowest position investigated, $z/d = 0.1$, a drastic increase in the peak heat transfer occurs. At the lowest spacing, $z/d = 0.1$, a local minimum in Nu is seen at the stagnation point and only a slight shoulder remains from the inner peak near $r/d \approx 0.5$, with the maximum heat transfer occuring at $r/d \approx 1.25$. It is interesting to note that the second peak or plateau in Nu shifts radially outward as z/d is increased. The inner peak (or shoulder as is sometimes seen for lower Re or z/d), however, remains fixed at $r/d \approx 0.5$ for all z/d spacings where it appears. These same trends are also seen, although less pronounced, at the lower Reynolds number, $Re = 5100$.

Little difference is seen between the radial Nusselt number profiles for nozzle–plate spacings of $z/d = 0.5$ and 6. The only difference is that the local data at $z/d = 0.5$ show a secondary peak at $r/d \approx 1.75$, whereas no such peak is seen in the local data for the larger spacing. Note, too, the general increase in heat transfer coefficient at all radial locations even for $z/d = 0.25$. While the acceleration of the *mean* flow in the nozzle–plate gap is induced for only $z/d < 0.25$, the *vena contracta* effect causes *local* acceleration effects,

resulting in higher heat transfer at this nozzle–plate spacing. This is corroborated by measurements of pressure drop, which revealed elevated pressure drop across the nozzle exit even for $z/d = 0.25$ [15].

Figure 7 illustrates the dependence of local Nusselt number on Reynolds number for dimensionless nozzle–plate spacings of 0.1 and 1.0. Aside from the obvious differences in the magnitudes of Nu for the same Reynolds number, the data show that the secondary maxima (or plateaus) in Nusselt number are more pronounced for smaller z/d. The secondary peaks in heat transfer coefficient can be nearly a factor of two higher than the stagnation point value for $z/d = 0.1$. Further, the data for $Re = 3600$ show that the outer peak in Nu and that normally associated with the acceleration in the nozzle–plate gap at $r/d = 0.5$ are nearly gone for the $z/d = 0.1$ case, and are virtually undetectable for $z/d = 1.0$. The data also show that the secondary maximum in Nu moves outward radially for higher Reynolds numbers.

The inner peaks in Nu have been explained here in terms of the increased convective heat transfer due to acceleration in the nozzle–plate gap. Figure 2 shows that the higher mean velocity (for low z/d) at $r/d = 0.5$ may also be accompanied by increases in the local level of RMS turbulence, which contributes to higher heat transfer coefficient as well. A review of prior work suggested that the presence and size of local maxima in Nusselt number near $r/d = 0.5$ is strongly dependent on nozzle geometry and Reynolds number [19].

The local heat transfer data indicate that the position of the outer peak is dependent upon Reynolds number and nozzle–plate spacing. Figures 8 and 9 illustrate radial profiles of the measured local Nusselt number and RMS turbulent fluctuations (u'/v_j) and radial turbulence intensity (u'/u) for the experimental conditions $z/d = 0.1$, 0.2, and 0.5 for $Re = 7800$ and

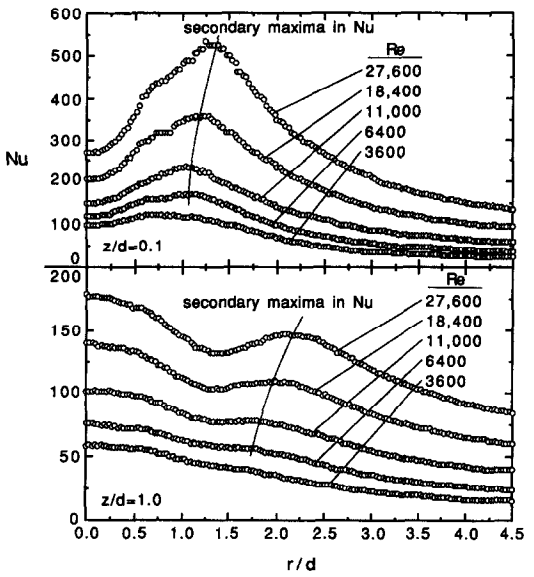

FIG. 7. Radial variation in Nusselt number with Reynolds number for two nozzle–plate spacings.

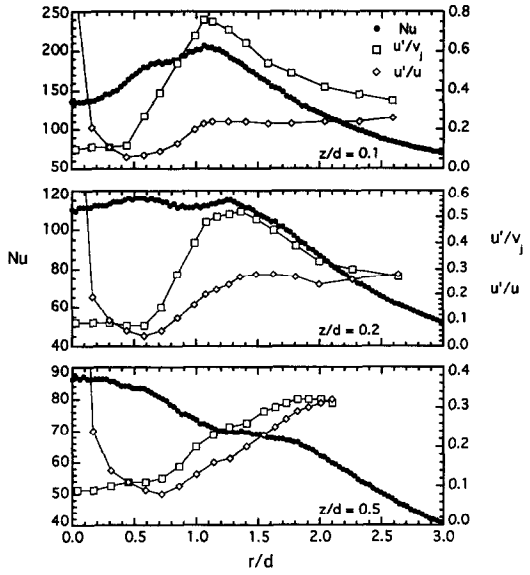

FIG. 8. Variation of local Nusselt number and RMS velocity fluctuation at $y/d = 0.05$ with radial location for $Re = 7800$, $d = 10.9$ mm.

11 000, respectively. These data were measured at a vertical position from the impingement plate corresponding to $y/d = 0.05$ and 0.025 for the $Re = 7800$ and 11 000 cases, respectively. The figures illustrate a definite correlation between the location of peak (or significantly increased) turbulence fluctuations and the point of outer maximum (or plateau) in the local Nusselt number. This correlation exists both with the absolute RMS turbulent fluctuations (u'/v_j) and the radial component of the turbulence intensity (u'/u). The conclusion is that the outer maximum (or plateau) in Nu is the result of significantly higher turbulence in the boundary layer which results from

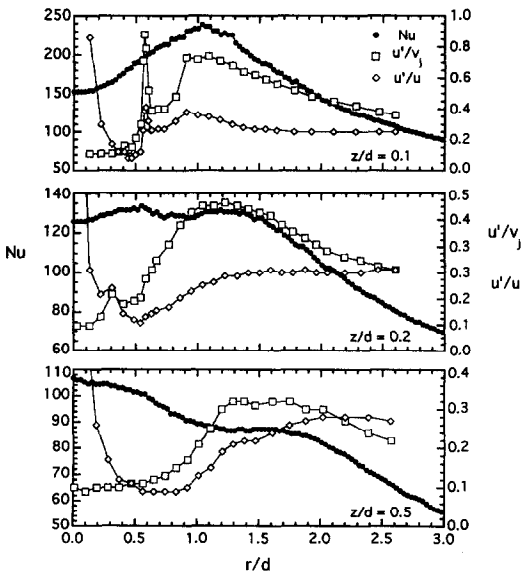

FIG. 9. Variation of local Nusselt number and RMS velocity fluctuation at $y/d = 0.025$ with radial location for $Re = 11\,000$, $d = 10.9$ mm.

intense shear between the radially exiting jet and the stagnant ambient at decreasing z/d. Since Fig. 6 shows that the radial location corresponding to outer peak Nuselt number decreases with reductions in z/d, it is speculated that acceleration at smaller spacings and the associated stronger shear interaction with the stagnant ambient may promote an increase in turbulence at lower r/d.

The radial location of the outer peaks in heat transfer coefficient discussed relative to the data of Figs. 6 and 7 was characterized in a previous paper [19]. The radial location of the peaks was found to increase with both Reynolds number and nozzle–plate spacing, following the relationship

$$(r/d)_{\text{sec max}} = 0.188Re^{0.241}(z/d)^{0.224}. \quad (10)$$

As was noted in the previous work, the dependence of the radial location of the secondary maximum in Nu is functionally influenced nearly identically by both Re and z/d.

It should be stressed that for nozzle–plate spacings less than $z/d = 0.25$ the maximum local heat transfer does not occur at the stagnation point but at a radial location of approximately $r/d \approx 1.0$–1.6, depending on nozzle–plate spacing and Reynolds number. A previous work concluded that there is a strong Reynolds number and nozzle–plate spacing dependence on the magnitude of the local heat transfer maximum, the greatest maximum occurring at small nozzle–plate spacings and high Reynolds numbers. Additionally, the secondary maximum gives way to a stagnation point maximum for $z/d \geqslant 0.25$.

It should be underlined that the significant increase in heat transfer coefficient for impinging jets at low nozzle–plate spacing is accompanied by a substantial increase in pressure drop through the system. Prior work has indicated that the fractional increase in pressure drop (over the free jet, for example) is significantly higher than the corresponding fractional increase in Nusselt number [19].

The average Nusselt number for the jet configurations investigated here was evaluated using equations (2) and (3). The same trends evident in the local data were also evident after averaging. The average Nusselt number evaluated at $r/d = 1.0$ and 2.0 for the range of nozzle–plate spacings $0.1 \leqslant z/d \leqslant 1.0$ and Reynolds numbers between 3600 and 27 600 were found, respectively, to be

$$\overline{Nu}_{r/d=1} = 0.424Re^{0.57}(z/d)^{-0.33} \quad (11)$$

and

$$\overline{Nu}_{r/d=2} = 0.150Re^{0.67}(z/d)^{-0.36}. \quad (12)$$

Equations (11) and (12) represent the experimental data with an average error of 9 and 8%, and a maximum error of 29 and 27%, respectively. Again, the strong dependence of heat transfer characteristics on z/d is illustrated for nozzle–plate spacings less than one diameter.

CONCLUSIONS

Air jet impingement for nozzle–plate spacings less than one nozzle diameter has been examined experimentally in the Reynolds number range $3600 \leqslant Re \leqslant 27\,600$. Flow structure measurements reveal significant increases in both mean velocity and RMS turbulence fluctuations as the nozzle–plate spacing is decreased. Wall pressure measurements corroborate the significant acceleration through the nozzle–plate gap for $z/d < 0.25$. Considerable heat transfer enhancement was observed due to global-continuity-forced acceleration of the impinging fluid as it escapes from the nozzle–plate gap, as well as significant increases in the turbulence level. These phenomena yield a stagnation point minimum and an inner and outer peak in the local heat transfer. It was seen that the outer peak, which was due to shear-induced increases in turbulence, moved radially outward for larger nozzle–plate spacings and larger Reynolds number flows. The inner peak disappeared for impingement spacings larger than $z/d = 0.25$. The location of the outer peak was found to coincide with a local maximum in turbulence fluctuations, suggesting considerably higher turbulent transport there.

Nusselt number results were correlated empirically and revealed functionally that stagnation point heat transfer coefficients increase significantly for decreasing nozzle–plate spacings. The experimental data were found to be represented quite well by an approximate analysis which was an extension of laminar theory for an impinging jet of infinite extent.

Acknowledgement—This work was sponsored by the U.S. National Science Foundation under Grant No. CBT-8552493.

REFERENCES

1. J. N. B. Livingood and P. Hrycak, Impingement heat transfer from turbulent air jets to flat plates—a literature survey, NASA TM x-2778 (1973).
2. S. J. Downs and E. H. James, Jet impingement heat transfer—a literature survey, ASME paper 87-HT-35, ASME, New York (1987).
3. H. Martin, Heat and mass transfer between impinging gas jets and solid surfaces. In *Advances in Heat Transfer* (Edited by J. P. Hartnett and T. F. Irvine), Vol. 13, pp. 1–60. Academic Press, New York (1977).
4. R. Gardon and J. C. Akfirat, The role of turbulence in determining the heat transfer characteristics of impinging jets, *Int. J. Heat Mass Transfer* **8**, 1261–1272 (1965).
5. S. P. Kezios, Heat transfer in the flow of a cylindrical air jet normal to an infinite plane, Ph.D. Thesis, Ill. Inst. of Tech. (1985).
6. B. N. Pamadi and O. A. Belov, A note on the heat transfer characteristics of a circular impinging jet, *Int. J. Heat Mass Transfer* **23**, 783–787 (1980).
7. C. J. Hoogendoorn, The effect of turbulence on heat transfer at a stagnation point, *Int. J. Heat Mass Transfer* **20**, 1333–1338 (1977).
8. E. M. Sparrow and T. C. Wong, Impingement transfer coefficients due to initially laminar slot jets, *Int. J. Heat Mass Transfer* **18**, 597–605 (1975).

9. M. T. Scholtz and O. Trass, Mass transfer in a non-uniform jet: Part 2. Boundary layer flow mass transfer, *A.I.Ch.E. Jl* **16,** 90–96 (1970).
10. R. J. Goldstein, A. I. Behbahani and K. K. Heppelmann, Streamwise distribution of the recovery factor and the local heat transfer coefficient to an impinging circular air jet, *Int. J. Heat Mass Transfer* **29,** 1227–1235 (1986).
11. B. R. Hollworth and L. R. Gero, Entrainment effects on impingement heat transfer: Part 2. Local heat transfer measurements, *ASME J. Heat Transfer* **107,** 910–915 (1985).
12. R. Gardon and J. Cobonpue, Heat transfer between a flat plate and jets of air impinging on it. In *International Developments in Heat Transfer*, pp. 454–460. ASME, New York (1965).
13. S. A. Striegl and T. E. Diller, An analysis of the thermal entrainment effect on jet impingement heat transfer, ASME Paper No. 82-WA/HT-54, ASME, New York (1982).
14. S. A. Striegl and T. E. Diller, The effect of thermal entrainment on jet impingement heat transfer, *ASME J. Heat Transfer* **106,** 27–33 (1984).
15. D. Lytle, Air jet impingement heat transfer at low nozzle-to-plate spacings, M.S. Thesis, Department of Mechanical Engineering, Brigham Young University, Provo, Utah, December (1990).
16. H. Schrader, Trocknung feuchter Oberflächen mittles Warmluftstrahlen Strömungsvorgänge und Stoffübertragung, *VDI Forscheft* **27B,** 484–498 (1961).
17. N. T. Obot, A. S. Majumdar, and W. J. M. Douglas, The effect of nozzle geometry on impingement heat transfer under a round turbulent jet, ASME Paper No. 79-WA/HT-53, ASME, New York, NY (1979).
18. L. C. Burmeister, *Convective Heat Transfer*. Wiley, New York (1983).
19. D. Lytle and B. W. Webb, Secondary maxima for air jet impingement at low nozzle-to-plate spacings, *Proceedings Second World Conference on Experimental Heat Transfer, Fluid Mechanics, and Thermodynamics* (Edited by J. F. Keffer, R. K. Shah and E. N. Gánic), pp. 776–783. Elsevier, New York (1991).